

RESPONSE TO REVIEWER'S COMMENTS

The paper needs to be reviewed by a native English speaker.

Response: The paper has been reviewed by Prof. Marin Clark, native English speaker, among others.

Generally, DSM or DEM concepts are used as synonymous, but DEM is the model of the terrain
1) Line 24: "Digital surface model (DSM) of the terrain". This sentence is not correct.

Response: DSM was replaced with DEM.

2) Keywords: DEM: DTM or DSM? "Restitution" what do you mean?

Response: Both DTM and DSM are used as keywords.

Restitution is the energy loss during impact of the falling rock.

3) Line 70: as line 24. No correct.

Response: DSM was replaced with DTM.

4) Figure 1 is still the previous one! The proposed new figure (with geological map) has not been replaced

Response: Figure 1 is not the previous one. We added a new Figure to localize the study area in Greece

5) Line 84: the correct definition is 800 m/s. sec doesn't exist!

Response: corrected

6) Figure 2 if the orthophoto of the site. It is quite difficult to see the "average slope" using this product. It is completely unhelpful. It is better to include the contour plots or making a 3D model.

Response: This Figure is presented in order to present the actual rockfall trajectory and indicate the source and end point of the rock. Subsequent figures are used to show slope.

7) Concerning the images or video. It is not declared the final GSD (ground sample distance). This parameter is fundamental working with digital images. Moreover, it is not declared the strategy adopted to collect the image or video. On photogrammetric point of view, which kind of flight plan have you adopted? It is necessary to include more detail about the data acquisition.

Response: Comments added at line 118-123

8) Figure 2 caption: study site is not correct: case study or test site.

Response: Corrected

9) In "introduction", 103-108, will be interesting to include an example of image. It is not clear if you have used the image or video. To be clarified

Response: 6 example images are shown in Fig. 5. As discussed in the text. Images were generated from the video

10) Line 113: replace wase with was

Response: ok

11) Line 114: the sentence is wrong. Using SfM you have generated a DSM. After, with a data processing, you have generated a DTM.

Response: Corrected

12) Line 115: replace imagery with imaery

Response: ok

13) Lines 122-128: you have to specify the GCPs' distribution and why you have chosen this distribution, how the GCPs' have been detected (manually or automatically), It is not clear the quality of the GSP.

Response: Not within the scope of this manuscript. Methodology described by Manousakis et al. (2016).

14) Line 128: "DSM or DTM". This is a mistake!! They are not synonymous!!

Response: This is not a mistake. Both were generated. DSM first. DTM next. This is now clarified in the text in line 116-117.

15) Line 128: replace orthophotos.

Response: It is not entirely clear what it is asked in this comment. Orthophotos were generated.

16) It is important to define the setting configuration of PHOTOSCAN, for alignment, point extraction etc. a summary table needs.

Response: Not within the scope of this manuscript

17) Line 134: " two surfaces were found to be very similar". It is necessary to declare the entity of the differences, considering max, min and mean values.

Response: A reference is made subsequently in the text, where quantitative assessment of the DEM from the UAV and the DEM of the Greek Cadastre are compared. Refer to Manousakis et al. (2016) for more details.

18) Figure 4 is completely unhelpful. It is necessary to include a more clear figure about the flight plan, showing the final foot print of the images.

Response: We believe that this figure shows nicely the pictures overlapping using SfM method and we would like to retain it. Since the overlap of the imagery is listed, and an orthophoto is also shown we do not believe a specific flight plan is necessary.

19) Figure 4 caption: replace Shematic with Schematic. This picture has to be completely replaced. It is terrible!

Response: We do not think it is terrible since it demonstrates in a perspective view the way a real object detail is identified and projected on several overlapping images.

20) Line 135-136: image or video? No clear. It is necessary to define how the camera has been calibrated and to summarize the calibration parameter in a table. Have you tried to calibrate the images with other methods?

Response: Video captured clarified. Precalibrated camera parameters by the SfM software (Photoscan) were introduced.

21) In the proposed correction there is a new figure 3 (about SFm) but in the paper is not included.

Response: We are not sure we understand this comment. Apologies.

22) In Figure 5, it is important to include a bar scale

Response: A scale was provided in the images in Figure 5

23) Line 159: "Noise filtering and smoothing processing" which one? Could you describe them? It could be better to include a flowchart of your process, with purpose to better understand your activity

Response: We provided more clarifications about the process

24) Line 165:"a bare-Earth digital" is a terrible sentence!

Response: We use this term to describe an intermediate step where the vegetation has already been removed, but not the structures. Thus, this DEM cannot be called DTM nor DSM.

25) In the proposed revision, you include the link of GAT tool, but it is not included in the uploaded version. To be included

Response: Reference included (line 182)

Lindsay JB. 2016. Whitebox GAT: A case study in geomorphometric analysis. Computers & Geosciences, 95: 75-84. DOI: 10.1016/j.cageo.2016.07.003

26) Have you verified the performance of the GAT tool? Have you compared your DTM with a DTM generated by a laser scanner?

Response: No, we have not. This was not a focus of our study.

27) Using this algorithm (OTO), is there the risk to remove also some rocks? Could you describe the parameter adopted in the filtering?

Response: There could be a risk involved there, since there is no straightforward process to only remove vegetation from an SfM point cloud. No process is perfect, but we do not think any errors here had a significant impact on the results.

28) Line 224: replace m/sec with m/s

Response: ok

29) Line 275: it is not clear why you have selected 2 case and the main differences. Please, to be clarify

Response: The comment is not clear

30) Line 356: In 2D and 3D analyses, I suggest to include a table where the initial parameters are summarized. It is very difficult to understand.

Response: Table 4 refers to the parameters of the 3D analysis. The authors believe that a Table is not necessary.

31) 2D analyses: it is not clear how the filtering (DSM to DTM) give some influence to the final results and simulation. Is it possible that some trees or bushes have been removed? What is the power of the vegetation filtering (min object).

Response: Yes, the objective is for the trees and bushes to be removed in the DTM. As explained in the text, we used the filtering, in combination with the imagery to try to reasonably identify ground. As the reviewer probably knows, no process is perfect, but we do not think any errors here had a significant impact on the results.

32) Figure 14 needs to be more explained.

Response: A sentence was added in line 413-414.

Reach probability is the percentage of the falling rocks along a given trajectory that reach a specific point along the line of the trajectory.

33) You declare in the conclusion that "...was successfully used". How can you define the "successful" of the system and method? It is not clear and described in the paper. It is necessary to define the quality of final result.

Response: UAV-enabled reconnaissance assisted in 1) identifying the exact position of the detachment point, which was inaccessible, 2) identifying the rolling section and the discrete impact points along the bouncing section of the trajectory and 3) creating an accurate model for 3D rockfall analysis.

34) Line 477: you declare that the 3D analysis is more accurate than 2D. how you can define this level of accuracy? In the paper is not well described this aspect. You have to be more clear.

Response: The level of accuracy is qualitative and is based on comparing the actual trajectory with those produced by the 3D modeling. The 2D modeling trajectory could not match the characteristics (type of motion, impact points) of the actual trajectory. 3D modeling did much better.

35) Considering the results, it seems that it is not possible to define the correct position of the origin, even considering your expertise and your knowledge. It is not clear the real benefits of the model generated with UAV with respect the public model or a global DTM generated with RS.

Response: The position of the origin of the rock was clearly detected using the UAV, as it would be impossible to reach this point in the field due to the presence of dense vegetation and due to the inaccessible nature of the detachment location on the cliff. The impact points and rolling section of the path were also clearly visible.. We believe that the developed model is of very high resolution, of reasonably high accuracy and generated very efficiently. We thus disagree with the reviewer's comment about the benefits of the model and find the reviewer's position biased.

36) References: check the references, because there are some incongruences (in some references pages are included in someone not, etc...)

Response: References were checked

UAV-based mapping, back analysis and trajectory modelling of a co-seismic rockfall in Lefkada Island, Greece

Charalampos Saroglou^{1*},

Pavlos Asteriou¹

Dimitrios Zekkos²

George Tsiambaos¹

Marin Clark³

John Manousakis⁴

¹Department of Geotechnical Engineering, School of Civil Engineering, National Technical University of Athens

²Department of Civil and Environmental Engineering, University of Michigan, USA

³Department of Earth and Environmental Science, University of Michigan, USA

⁴Elxis Group, S.A, Athens, Greece

* corresponding author: saroglou@central.ntua.gr

Abstract

We present field evidence and a kinematic study of rock block motion mobilised in the Ponti area by a ~~M_w~~ ~~6.5~~ earthquake near the island of Lefkada on 17th November 2015. A detailed survey was conducted using an Unmanned Aerial Vehicle (UAV) with an ultra-high definition (UHD) camera, which produced a high-resolution orthophoto and a Digital Elevation-Terrain Model (DEMDTM) ~~of the terrain~~. The sequence of impact marks from the rock trajectory on the ground surface was identified from the orthophoto and field verified. ~~Additionally, calculation of~~ Eearthquake characteristics ~~defined were used to estimate~~ the acceleration of the rock slope and the initial condition of the detached block. Using the impact points from the measured rockfall trajectory, an analytical reconstruction of the trajectory was ~~developed~~ undertaken, which led to insights on the coefficients of restitution. The

31 measured trajectory was compared with modeled rockfall trajectories using
32 recommended parameters. However, the actual trajectory could not be accurately
33 predicted, revealing limitations of existing rockfall analysis software models used in
34 engineering practice.

35 **Keywords**

36 Rockfall, earthquake, DSM DSM, DTM, modelling, restitution, UAV

37 **1. Introduction**

38 Active faulting, rock fracturing and high rates of seismicity contribute to ~~common a~~
39 high rockfall hazards in Greece. Rockfalls primarily damage roadways and houses
40 (Saroglou, 2013) and are most often triggered by rainfall and, secondly, seismic
41 loading. ~~Additionally In~~ recent years, some rockfalls have impacted archaeological
42 sites (Marinos & Tsiambaos, 2002, Saroglou et al., 2012). The Ionian Islands, which
43 include Lefkada Island, experience frequent M_w 5-6.5 earthquakes, as well as less
44 frequent larger (up to 7.5) earthquakes. The historical seismological record for the
45 island is particularly well constrained with reliable detailed information for at least 23
46 such earthquake events ~~since 1612~~ that induced ground failure since 1612s at the
47 island of Lefkada. On average, Lefkada experiences a damaging earthquake every
48 18 years. In the recent past, a M_w 6.2 earthquake occurred on August 14 2003
49 offshore the NW coast of Lefkada, and caused landslides, rockslides and rockfalls
50 along the western coast of the island (Karakostas et al. 2004, Papathanasiou et al.,
51 2012). Significant damage was reported, particularly in the town of Lefkada, where a
52 PGA of 0.42g was recorded.

53 On November 17th 2015, an M_w 6.5 earthquake ~~again~~ struck the island of Lefkada
54 and triggered a number of landslides, rockfalls and some structural damage. The
55 most affected area by large rockslides was the western coast of the island, especially
56 along its central and south portion, which are popular summer tourist destinations

57 (Zekkos et al., 2017). The coseismic landslides completely covered the majority of
58 the west coast beaches and damaged access roads.

59 On the southeast side of Lefkada, near the Gulf of Vassiliki, a seismically-triggered
60 rockfall in Ponti village was responsible for one of two deaths caused by the
61 earthquake (Figure 1). Of particular interest, is the very long travel path of the rock
62 block, which was about 800 m in plan view from the point of detachment to the end of
63 its path. Near the end of the rock fall path, the block impacted a family residence,
64 penetrated two brick walls and killed a person in the house. The block exited through
65 the back of the house and came to rest in the property's backyard.

66 The Ponti village rockfall site is a characteristic ~~of earthquake-induced rockfall and an~~
67 example of how seismically-induced rockfalls s impacts human activities. It also
68 provides an opportunity to evaluate 2D and 3D rockfall analysis to predict details of
69 the rockfall trajectory, based on ~~measured-by~~ field evidence. In order to create a
70 highly accurate model of the rockfall propagation in 2D and 3D space, the rock path
71 and the impact points s on the slope ~~were~~ identified by a field survey. The study was
72 performed using an Unmanned Aerial Vehicle (UAV) with an ultra-high definition
73 (UHD) camera, which produced a high-resolution orthophoto and a Digital Elevation
74 Terrain Model (DEMDTM) of the ~~terrainslope~~. The orthophoto was used to identify
75 the rolling section and the ~~bouncing-impact~~ points of the rock along its trajectory,
76 which were verified by field observation. The high-resolution DSMDTM made it
77 possible to conduct kinematical rebound analysis and a 3D rockfall analysis.

78 **2. Ponti rockfall - site conditions**

79 The locations of the epicenters of the 2003 and 2015 events, as well as the location
80 of the rockfall ~~case study-site~~ are shown in Figure 1. The southwest coast of Lefkada
81 is part of the Triassic to Eocene age Paxos zone and consists of limestones and
82 dolomites that are covered by Neogene clastic sedimentary rocks, mostly sandstones

83 and marls. Figure 1 also shows faults and high rockfall hazard areas as identified by
84 Rondoyanni et al. (2007). The rockfall at Ponti is not located in an identified high
85 rockfall hazard area. Based on measurements conducted at one location along the
86 rockfall path using the Multichannel Analysis of Surface Waves method, the in-situ
87 shear wave velocity of the top layer was estimated to be around 800 m/s, which is a
88 high velocity and is consistent with the limestone rock ~~rock conditions expected~~ at the
89 site.

90 The slope overhanging Ponti village (shown in Fig. 2) ~~is made of limestone and~~ has
91 a maximum height of 600 m and an average slope angle of 35° to 40° ~~(Figure 2)~~. The
92 geological formations at the Ponti rockfall site are limestones covered by moderately
93 cemented talus materials. The thickness of the talus materials, when present, ranges
94 between 0.5 and 4.0 ~~to 5.0~~ m. ~~A few~~ Several detached ~~fallen~~ limestone blocks were
95 identified on the scree slope, with volumes between 0.5 and 2 m³. Based on the size
96 distribution of these rocks on the slope, the average expected block volume would be
97 in the order of 1 to 2 m³.

98 The rockfall release area was at an elevation of 500 m, while the impacted house
99 (shown in Figure 3) at an elevation of 130 m ~~(Figure 3)~~. The volume of the detached
100 limestone block was approximately 2 m³ and its dimensions equal to 1.4 m x 1.4 m x
101 1 m. There was no previously reported rockfall incident ~~reported for the specific~~
102 ~~slope at Ponti~~ that impacted the road or a house.

103 **3. UAV mapping**

104 **3.1. Introduction**

105 A quadrotor UAV (Phantom 3 professional) was deployed to reach the uphill terrain
106 that was practically inaccessible. The UAV was equipped with an Ultra-high definition
107 (UHD) 12 MP camera and had the capacity to collect 4K video. The sensor was a
108 1/2.3" CMOS (6.47x3.41mm) and the effective pixel resolution was 12.4 MP

109 (4096x2160 pixels). An immediate UAV data acquisition expedition was conducted 2
110 days after the earthquake. A second more detailed mapping UAV expedition with the
111 objective to create a [DEM-DTM](#) was conducted 5 months after the rockfall event.

112 The first objective of the UAV deployment was to find the initiation point of the rock
113 and then identify the rockfall path (shown in Figure 2). A particular focus on that part
114 of the task was the identification of rolling and bouncing sections of the rockfall path.

115 In addition, ~~in order~~ to generate a high-resolution orthophoto of the rockfall trajectory,
116 aerial video imagery was collected, and the resulting digital surface model (DSM)
117 [and digital terrain model \(DTM\)](#) was used to perform rockfall analysis.

118 [The aerial survey was conducted by capturing 4K video along a gridded pattern](#)
119 [covering the area of interest, at a mean flight altitude of 115m above the terrain](#)
120 [resulting image frames of a mean ground sampling distance \(GSD\) of](#)
121 [4.97cm/pix. The overlap between image frames was minimum frontal 80%,](#)
122 [side 65% and a total of 714 camera stations \(video frames extracted\) were included](#)
123 [as shown in Figure 4.](#)

124 The Structure-from-Motion (SfM) methodology was implemented to create a 3D
125 point cloud of the terrain and develop a 3D model. The methodology is based on
126 identifying matching features in multiple images, and thus imagery overlap of at least
127 70% is required. Compared to classic photogrammetry methodologies, where the
128 location of the observing point is well established, SfM tracks specific discernible
129 features in multiple images, and through non-linear least-squares minimisation
130 (Westoby et al., 2012), iteratively estimates both camera positions, as well as object
131 coordinates in an arbitrary 3D coordinate system. In this process, sparse bundle
132 adjustment (Snavely et al., 2008) is implemented to transform measured image
133 coordinates to three dimensional points of the area of interest. The outcome of this
134 process is a sparse 3D point cloud in the same local 3D coordinate system
135 (Micheletti et al., 2015). Subsequently, through an incremental 3D scene

136 reconstruction, the 3D point cloud is densified. Paired with GPS measurements of a
137 number of control points (for this site, 10 fast-static GPS points were collected) at the
138 top, middle and bottom of the surveyed area, the 3D point cloud is georeferenced to
139 a specific coordinate system and through post-processing a digital surface model
140 (DSM), ~~or a~~ digital terrain model (DTM) and orthophotos are created. The SfM
141 methodology was implemented in this study using the Agisoft Photoscan software.
142 Precalibrated camera parameters by the SfM software (Photoscan) were introduced
143 and then optimized during the matching process and the initialization of Ground
144 Control Points.

145 In addition, the accuracy of the model has been examined by using portions of the
146 ground control points and developing DEM-DTM of differencing between different
147 models, an investigation that is described ~~in our paper~~ by Manousakis et al. (2016).
148 Finally, a comparison was made of the DEM-DTM developed by the UAV against the
149 satellite-based DEM-DTM that is part of the used for the Greek cadastre. The two
150 surfaces were found to be very similar, as discussed subsequently.

151 ~~The overlap between pictures was minimum frontal 80%, side 65% and a total of 714~~
152 ~~camera station (video frames extracted) were included as shown in Figure 4.~~

153 **3.2. High-resolution Orthophoto**

154 A 5cm pixel size orthophoto was generated based on the methodology outlined
155 earlier. As shown in Figure 5, the rolling section and the bouncing locations of the
156 rock block throughout its course were identified. The rolling section was easily
157 discerned as a continuous and largely linear mark left in the ~~densely~~ vegetated
158 terrain ~~that was indicative of the damage caused~~. Impact points that are part of the
159 bouncing section of the rock, were identified as circular to ellipsoidal bare earth
160 craters with no disturbance in between. The last bouncing point before impacting the
161 house is clearly identified on the paved road. The plan view ortho-imagery, along with
162 the original footage of the video collected was crucial to the qualitative identification

163 of these features. The alternative, i.e., land-based, conventional field reconnaissance
164 was physically impossible to perform ~~throughout the in the densely~~ vegetated and
165 steep terrain.

166 3.3. Digital Surface Model and Digital Terrain Model

167 A profile section and a 10 cm Digital Surface Model (DSM) ~~paired with the plan view~~
168 ~~orthophoto~~ were ~~then first~~ developed (Manousakis et al., 2016) allowing the
169 identification of ~~terrain~~ features such as structures, slope benches or high trees,
170 which could affect the rock's path downhill. ~~However~~ Subsequently, this resolution of
171 the DSM proved to be not only unnecessarily high and thus difficult to manipulate in
172 subsequent rockfall analyses, but also ~~caused resulted in~~ numerical instabilities in
173 ~~during~~ the rockfall analyses. Therefore, a downscaled 2 m DTSM was produced for
174 the rockfall analysis as described next. First, . ~~This was implemented through an~~
175 aggregate generalization scheme where each output cell is assigned the minimum
176 elevation of the input cells that are encompassed by that cell. In addition, noise
177 filtering and smoothing processing were implemented to reduce the effect of
178 ~~construction elements and~~ vegetation in the final rasterized model. Note that this
179 resolution is still higher than the resolution of DSM-DTM that are often used in
180 rockfall analyses.

181 To create the DTM, a Algorithms for vegetation removal were executed using within
182 Whitebox GAT Geospatial Analysis Tools platform (Lindsay, 2016) . ~~GCPs were~~
183 used for both georeferencing and solving camera's internal and external parameters.
184 The process involves Point Cloud neighborhood examination and DEM smoothing
185 algorithms. Firstly, a bare-Earth digital elevation model (DEM) was interpolated from
186 the input point cloud LAS file, by specifying the grid resolution (2m) and the inter-
187 point slope threshold. The algorithm distinguished ground points from non-ground
188 points based on the inter-point slope threshold. Thus, T the interpolation area was
189 divided into grid lattice cells, corresponding to the cells grid of the output DEM. All of

190 the point cloud points within the circle ~~encompassing~~ containing each grid cell were
191 then examined as a neighborhood. ~~All-Those~~ points within a neighborhood that have
192 an inter-point slope with any other point and are also situated above the
193 corresponding point, are ~~considered to be attributed as~~ non-ground points. An
194 appropriate value for the inter-point slope threshold parameter depends on the
195 steepness of the terrain, but generally values of 15-35 degrees produce D satisfactory
196 results. The elevation assigned to the grid cell was then the nearest ground point
197 elevation (Lindsay, 2016.).

198 Further processing of the interpolated bare-earth DEM was ~~introduced~~ executed to
199 improve vegetation and structures removal results by applying a second algorithm to
200 point cloud DEMs, which frequently contain numerous off-terrain objects such as
201 buildings, trees and other vegetation, cars, fences and other anthropogenic objects.
202 The algorithm works by ~~finding~~ locating and removing steep-sided peaks within the
203 DEM. All peaks within a sub-grid, with a dimension of the user-specified Maximum
204 Off-Terrain Object (OTO) Size, in pixels, were identified and removed. Each of the
205 edge cells of the peaks were then ~~examined~~ queried to ~~see~~ check if they had a slope
206 that is less than the user-specified Minimum OTO Edge Slope and a back-filling
207 procedure was used. This ensured that ~~OTOs are distinguished from~~ natural
208 topographic features such as hills are not recognized and confused as Off-Terrain
209 features. (Whitebox GAT help topics).

210 The final DTM model had a tTotal RMS error after filtering for 6 GCPs was 0.07m,
211 while total RMS error for 4 Check Points was 0.20m. When compared to a 5m DEM
212 from Greek National Cadastre with a geometric accuracy of $RMSE_z \leq 2,00m$ and
213 absolute accuracy $\leq 3,92m$ for a confidence level of 95%, a mean difference of 0.77
214 m and a standard deviation of 1.25 m is observed, which is well into the range of
215 uncertainty of the cadastre model itself.

216

217 **4. Earthquake characteristics – Initial conditions**

218 **4.1. Seismic acceleration**

219 The epicenter of the earthquake according to the National Observatory of Athens,
220 Institute of Geodynamics (NOA) is located onshore near the west coast of Lefkada.
221 The causative fault is estimated to be a near-vertical strike-slip fault with dextral
222 sense of motion (Ganas et al., 2015, 2016). Based on the focal mechanism study of
223 the earthquake, it was determined that the earthquake was related to the right lateral
224 Kefalonia-Lefkada Transform Fault (KLTF), which runs nearly parallel to the west
225 coasts of both Lefkada and Kefalonia island, in two segments (Papazachos et al.
226 1998, Rondoyanni et al. 2012).

227 A strong motion station recorded the ground motions in the village of Vasiliki located
228 at a distance of 2.5 km from the Ponti rockfall site. The ground motion characteristics
229 of the recording are summarized in Table 1 and are presented in Figure 6, ~~according~~
230 ~~to an ITSAK preliminary report~~ (ITSAK, 2016).

231 **4.2. Topography effect**

232 Peak ground acceleration (PGA) along the rock slope is estimated from the PGA of
233 the the intensity of base shaking (PGA_b) modified by site and topographic effects
234 (Mavrouli et al., 2009). In the present case, local shaking intensity in terms of
235 horizontal PGA was considered. The E-W component of acceleration was considered
236 for the determination of the initial velocity. The peak ground acceleration (~~PGA~~) on
237 the slope face (PGA_{sf}) was considered equal to the acceleration at the slope crest
238 (PGA_{cr}). The acceleration at the base was equal to 0.32g and thus at the crest
239 $PGA_{cr} = 1.5 PGA_b$ was equal to 0.48g.

240 **4.3. Initial velocity of rock block**

241 The initial horizontal velocity of the block, at the time of detachment, was calculated
242 considering equilibrium of the produced work and the kinetic energy according to
243 equation 1.

$$244 \quad v_x = \sqrt{2 \times PGA_{sf} \times s} \quad (1),$$

245 where PGA_{sf} is the acceleration on the slope at the location of detachment and s the
246 initial displacement of the block in order to initiate its downslope movement.

247 The initial horizontal velocity was calculated equal to 0.67 m/s, considering a
248 displacement in the order of $s = 0.05$ m. The vertical component of the initial velocity
249 is assumed to be zero.

250 **5. Trajectory analysis**

251 In order to estimate the possible rock paths and design remedial measures,
252 simulation programs based on lumped-mass analysis models are commonly used in
253 ~~engineering design~~-practice. The trajectory of a block is modelled as a combination of
254 four motion types; free falling, bouncing, rolling and sliding (Descoedres and
255 Zimmermann, 1987). Usage of the lump-mass model has some key limitations; the
256 block is described as rigid and dimensionless with an idealized shape (sphere);
257 therefore the model neglects the block's actual shape and configuration at impact,
258 even though ~~it is evident that they~~ both affect the resulting motion.

259 **5.1. Modelling the response to an impact**

260 The most critical input parameters are the coefficients of restitution (COR), which
261 control the bouncing of the block. In general, the coefficient of restitution (COR) is
262 defined as the decimal fractional value representing the ratio of velocities (or
263 impulses or energies; depending on the definition used) before and after an impact of
264 two colliding entities (or a body and a rigid surface). When in contact with the slope,
265 the block's magnitude of velocity changes according to the COR value. Hence, COR
266 is assumed to be an overall value that takes into account all the characteristics of the

267 impact; including deformation, sliding upon contact point, transformation of rotational
268 moments into translational and vice versa (Giani, 1992).

269 The most widely used definitions originate from the theory of inelastic collision as
270 described by Newtonian mechanics. For an object impacting a rocky slope (Figure 7),
271 which is considered as a steadfast object, the kinematic COR (v_{COR}) is defined
272 according to Eq. 2.

$$273 \quad \underline{v_{COR}} = \frac{v_r}{v_i} \quad (2)$$

274 where v is the velocity magnitude and the subscripts i and r denote the trajectory
275 stage; incident (before impact) and rebound (after impact) respectively.

276 Two different mechanisms participate in the energy dissipation process; energy loss
277 normal to the slope is attributed to the deformation of the colliding entities, and in the
278 tangential direction is due to friction between them. Therefore kinematic COR has
279 been analyzed to the normal and tangential component with respect to the slope
280 surface, defining the normal (n_{COR}) and the tangential (t_{COR}) coefficient of restitution
281 (Eq. 3 and 4 respectively).

$$282 \quad \underline{n_{COR}} = \frac{v_{n,r}}{v_{n,i}} \quad (3)$$

283 and

$$284 \quad \underline{t_{COR}} = \frac{v_{t,r}}{v_{t,i}} \quad (4)$$

285 where the first subscript, n or t denotes the normal or the tangential components of
286 the velocity respectively.

287 Normal and tangential COR have prevailed in natural hazard mitigation design via
288 computer simulation due to their simplicity. Values for the coefficients of restitution
289 are acquired from values recommended in the literature ([e.g., Azzoni et al. 1995](#);

290 Heidenreich 2004; Richards et al. 2001, RocScience, 2004). ~~These~~ values are
291 mainly related to the surface material type and originate from experience,
292 experimental studies or back analysis of previous rockfall events. This erroneously
293 implies that coefficients of restitution are material ~~constants~~properties. However,
294 COR values depend on several parameters that cannot be easily assessed.
295 Moreover, ~~the~~ values suggested in the literature~~by different authors~~ vary considerably
296 and are sometimes contradictory.

297 **5.2. Rockfall path characteristics**

298 23 impact points were identified on the slope surface (Figure 8). Their coordinates
299 are presented in Table 2, along block's path starting from the detachment point
300 (where $x=0$). No trees were observed along the block's path.

301 The apparent dip of the slope at impact positions was measured from the DTM
302 ~~topographic map~~; on each impact point a line was set with a length twice the block's
303 mean dimension, oriented according to preceding trajectory direction. Moreover, the
304 impact point was expanded on the ~~topographic map~~DTM to a rectangular plane with
305 a side twice ~~as much~~ the mean dimension of the block (Figure 9). This plane was
306 then oriented so that one side coincides with the strike direction and its' vertical side
307 ~~towards~~to the dip direction. Thus, direction difference, $\Delta\phi$, was measured by ~~the~~
308 strike direction and the preceding path and deviation, e , was measured as the angle
309 between ~~pre-~~ and ~~post-~~ impact planes (Asteriou & Tsiambaos, 2016).

310 Having a detailed field survey of the trajectory path, a back analysis according to the
311 fundamental kinematic principles was performed with the intent~~in order~~ to back-
312 calculate the actual COR values.

313 **5.3. Kinematic analysis and assumptions**

314 The 23 impact points identified on the slope comprise a rockfall path of 22 parabolic
315 segments. The vertical and horizontal length of each segment is acquired by

316 subtracting consecutive points. Since no external forces act while the block is ~~in the~~
317 ~~mid-air~~, each segment lays on a vertical plane and is described by the general
318 equation of motion as:

$$319 \quad \underline{y = x \tan \vartheta - \frac{gx^2}{2v_i^2 \cos^2 \vartheta}} \quad (5)$$

320 where: θ the launch angle from the horizon and v the launch (initial) velocity (Figure
321 10).

322 Since no evidence can be collected regarding launch angle and velocity, innumerable
323 parabolas satisfy Eq. 5. However, θ is bound between $-\beta$ and 90° , so in order to
324 acquire realistic values for the initial velocity, its sensitivity for that given range was
325 ~~addressed_invesstigated(Figure 11)~~.

326 For the case presented in Fig. 11 (the first parabolic segment) it is ~~shown~~ that for
327 the majority of the release angles, initial velocity variation is low and ranges between
328 7.2 and 12 ms^{-1} . Additionally, the relationship between release angle and initial
329 velocity is expressed by a curvilinear function, ~~withthus~~ a minimum initial velocity
330 value along with ~~itsan associated~~ release angle (denoted hereafter as θ_{cr}) ~~can be~~
331 ~~easily acquired~~.

332 Given the minimum initial velocity and the critical release angle for each parabolic
333 segment, the impact velocity and impact angle can be calculated.
334 ~~SubsequentlyAfterwards,~~ normal and tangential velocity components according to
335 the apparent dip of the impact area, are calculated in order to evaluate COR values.
336 Results are summarized in Table 3.

337 **5.4. Coefficients of restitution**

338 It is observed that v_{cor} (Table 3) is ~~slightly~~ greater than one in 5 out of 22 impacts.
339 According to Eq. 3, this can only be achieved when impact velocity is less than
340 rebound velocity. However, this indicates that energy was added to the block ~~upon~~

341 ~~impact during contact~~, which is not possible according to the law of conservation of
342 energy. Thus, impact velocity should be greater, which is possible if the launch
343 velocity of the previous impact was ~~higher~~ ~~more~~ than the assumed minimum.

344 ~~Omitting the impacts with~~ For the cases where $V_{cor} \leq 1$, it is observed that kinematic
345 COR ranges between 0.55 and 1.0 and presents smaller variation compared to
346 normal or tangential coefficient of restitution, similar to what was previously reported
347 in relevant literature (i.e. Asteriou et al, 2012; Asteriou & Tsiambaos, 2016).

348 The ~~considerably~~ wide scatter of normal COR implies that the restitution coefficient
349 cannot be a material constant. Yet, in most relevant software, normal COR is defined
350 solely by the slope material. Moreover, normal COR values higher than one were
351 calculated in 11 out of the 15 remaining impacts. Normal COR higher than one have
352 been observed in both experimental (e.g. Spadari et al., 2011; Buzzi et al., 2012;
353 Asteriou et al., 2012) and back-analysis studies (e.g. Paronuzzi, 2009) and are
354 related to irregular block shape and slope roughness, as well as to shallow impact
355 angle and angular motion. A more detailed presentation of the reasons why normal
356 COR exceeds unity can be found in Ferrari et al. (2013). However, in rockfall relevant
357 software used in engineering practice, normal COR values are bounded between 0
358 and 1.

359 ~~Moreover, it is observed~~ As shown in Figure 12 ~~that~~, normal COR increases as the
360 impact angle reduces, similarly to previous observations by Giacomini et al. (2012),
361 Asteriou et al. (2012) and Wyllie (2014). The correlation proposed by Wyllie (2014) is
362 also plotted in Figure 13 and seems to describe consistently, but on the
363 unconservative side, the trend and the values acquired by the aforementioned
364 analysis and assumptions.

365 **6. Rockfall modelling**

366 **6.1. 2-D analyses**

367 ~~Initially, a~~ deterministic 2D rockfall analysis was first performed using Rocfall
368 software (RocScience, 2004). According to Asteriou & Tsiambaos (2016) the most
369 important influence is posed by the impact configuration, which is influenced by slope
370 roughness and block shape. In this study, roughness has been fully taken into
371 account (considering the block's dimension scale) by the high resolution of accurate
372 the cross-section used in the analyses (more than 1500 x-y points were used –
373 approximately 2 points per meter). Based on our experience, this resolution accuracy
374 is significantly higher compared to other rockfall studies similar research projects.
375 Moreover, ~~with the available data and the performed lump-mass model analysis,~~ it
376 was not possible to simulate block shape effect, nor the configuration of the block at
377 impact, using lumped-mass model analysis.

378 Considering an initial velocity of 0.67 m/sec, according to the numerical analyses, the
379 falling rock primarily rolls on the slope and stops much earlier than its actual (field-
380 verified) run out distance, approximately 400 m downslope from its initiation starting
381 point (Fig. 8; case 1). The restitution coefficients were $n_{COR}=0.35$, $t_{COR}=0.85$, and
382 were selected based on which represent properties of bedrock outcrops according to
383 the suggested values for bedrock outcrops provided in the software documentation
384 of the software.

385 Note that for this analysis, ~~t~~The friction angle was set to zero. A standard deviation
386 for the coefficients of restitution, the friction angle and roughness of the material on
387 the slope was not used, ~~as the for this deterministic analysis was deterministic.~~ For
388 ~~the~~ friction equal to angle is set to $\varphi=32^{\circ}$ (as suggested by the software
389 documentation), the rock travels downslope only 50 m.

390 ~~Additional separate~~ analysis was also performed, with lower coefficients of restitution
391 that are representative of, ~~resembling that of the~~ talus material on the slope
392 ($n_{COR}=0.32$, $t_{COR}=0.82$, $\varphi=30^{\circ}$) per as proposed by the suggested values provided in
393 the software documentation ~~of the software~~. In this case, the rock block rolled only a

394 few meters downslope. Therefore, it is evident that the actual rock trajectory cannot
395 be simulated.

396 In order to more closely simulate the actual trajectory ~~as much as possible~~, various
397 combinations of restitution coefficients and friction angle were considered. The
398 closest match occurred for $n_{COR}=0.60$ and $t_{COR}=0.85$, while the friction angle was set
399 to zero and no velocity scaling was applied. ~~For these input parameters~~ Only in such
400 ~~an analysis~~, the rock block reaches the house; ~~with a velocity of equal to $v=18$ m/s~~
401 approximately (Fig. 8; case 2). ~~According to the suggested values, t~~ these values for
402 the restitution coefficients correspond to a bedrock material (limestone).

403 In this case, the modelled trajectory is significantly different from the actual one. The
404 main difference is that the block ~~is rolling~~ is rolling up to 200 m downslope while the actual
405 rolling section is 400 m (as shown in Figure 8). Furthermore the impacts on the
406 ground in the bouncing section of the trajectory are considerably ~~fewer~~ different in
407 number (14 versus 23) and in different ~~locations compared to from~~ the actual ones.
408 Finally, the bounce height of some impacts seems unrealistically high. For example,
409 the 2nd bounce ~~has presents~~ has presents a jump height (f) of ~ 17.5 m over a length (s) of ~ 50 m,
410 resulting to a f/s ratio of $\sim 1/3$, when the characteristic f/s ratios for high, normal and
411 shallow jumps is $1/6$, $1/8$ and $1/12$ respectively, as suggested by Volkwein et al.
412 (2011).

413 **6.2. 3-D rockfall analysis**

414 The rockfall trajectory model Rockyfor3D (Dorren, 2012) has also been used in order
415 to validate the encountered trajectory and ~~assess~~ assess ~~determine~~ the ~~reach~~ reach probability
416 ~~that~~ that the falling rock (from the specific source area) ~~on reaches~~ on reaches the impacted house.

417 The 3D analysis was based on the down-scaled 2 m resolution Digital Elevation
418 Terrain Model (DEM/DTM) that was generated from the 10 cm DSM. ~~The terrain~~
419 ~~features such as low vegetation (e.g. bushes) and the trees were removed from the~~

420 ~~DEM as they affected the rock's path downhill.~~The following raster maps were
421 developed for the 3D analysis: a) rock density of rockfall source, b) height, width,
422 length and shape of block, c) slope surface roughness and d) soil type on the slope,
423 which is directly linked with the normal coefficient of restitution, n_{COR} .

424 The slope roughness was modeled using the mean obstacle height (MOH), which is
425 the typical height of an obstacle that the falling block encounters on the slope at a
426 ~~possibility percentage~~ probability of 70%, 20% and 10% of the trajectories (according
427 to the suggested procedure in Rockyfor3D). No vegetation was considered in the
428 analysis, which favours a longer trajectory. The parameters considered in the 3D
429 analysis for the different formations are summarised in Table 4. The spatial
430 occurrence of each soil type is shown in Figure 13 and the assigned values of n_{COR}
431 are according to the Rockyfor3D manual. The values for soil type 4.1 in Figure 13 are
432 slightly different from those of soil type 4 (proposed in the manual), denoting talus
433 with a larger percentage of fallen boulders. The block dimensions were considered
434 equal to 2 m^3 and the shape of the boulder was rectangle. In order to simulate the
435 initial velocity of the falling rock due to the earthquake, an additional initial fall height
436 is considered in the analysis, which for this case was set equal to 0.5 m.

437 The energy line angles were recalculated from the simulated trajectories and it was
438 determined that the energy line angle with highest frequency (39%) was $30\text{-}31^\circ$.
439 Based on the 3D analysis no rock blocks would impact the house, although the rock
440 paths are closer to the actual trajectories compared to RocFall software. The reach
441 probability of the falling rocks, initiating from the source point, is shown in Figure 14.
442 Reach probability is the percentage of the falling rocks in relation to the total number
443 of falling rocks that reach a specific point along the line of the trajectory.

444 **6.3. Lateral dispersion & Deviation**

445 Lateral dispersion is defined as the ratio between the distance separating the two
446 extreme fall paths (as seen looking at the face of the slope) and the length of the

447 slope (Azzoni and de Freitas 1995). According to Crosta and Agliardi (2004) the
448 factors that control lateral dispersion are ~~(a) classified in three groups:~~ macro-
449 topography factors, factors related to the overall slope geometry; ~~(b)~~ micro-
450 topography factors controlled by the slope local roughness; and ~~(c)~~ dynamic factors,
451 associated with the interaction between slope features and block dynamics during
452 bouncing and rolling. ~~Based on Assessing the results of an~~ experimental
453 investigation, Azzoni and de Freitas (1995) ~~commented~~noted that the dispersion is
454 generally in the range of 10% to 20%, regardless of the length of the slope and that
455 steeper slopes ~~present~~ exhibit smaller dispersion. Agliardi and Crosta (2003)
456 calculated lateral dispersion to be up to 34%, ~~using~~via high-resolution numerical
457 models on natural rough and geometrically complex slopes.

458 Lateral dispersion cannot be defined from the actual rockfall event in Ponti since only
459 one path is available. Using the simulated trajectories from RockyFor3D, which are in
460 the 3d space (Figure 15), a lateral dispersion of approximately 60% is shown in the
461 middle of the distance between detachment point and the house. This is significantly
462 higher ~~dispersion than compared to~~ the findings of Azzoni and de Freitas (1995) and
463 Agliardi and Crosta (2003). ~~Moreover, based on the actual event and intuition, t~~The
464 lateral dispersion computed by RockyFor3D is extremely pronounced and most likely
465 due to the topography effect of the area of detachment. Specifically, the origin of the
466 rock block is located practically on the ridgeline, facilitating the deviation of the rock
467 fall trajectory from the slope line. ~~Examining Figure 15, it is notable that the rock~~
468 ~~paths are severely affected by topography. Therefore, assessing lateral dispersion~~
469 ~~seems to be a case specific task.~~

470 Asteriou & Tsiambaos (2016) defined deviation (e) as the dihedral angle between the
471 pre- and post-impact planes that contain the trajectory. They found that deviation is
472 controlled by the direction difference $\Delta\phi$, the slope inclination and the shape of the
473 block. For a parallel impact (i.e. $\Delta\phi=0^0$) a spherical block presents significantly less

474 deviation compared to a cubical. Additionally, deviation is equally distributed along
475 the post-impact direction and reduces as the slope's inclination increases. On oblique
476 impacts, the block's direction after impact changes towards the slope aspect
477 and as $\Delta\phi$ increases, this trend becomes more pronounced.

478 Figure 16 illustrates the relationship of deviation with a function of
479 direction difference. It is noted that for parallel impacts ($\Delta\phi=0^\circ$), deviation is uniformly
480 also equally distributed along the post-impact direction. As direction difference
481 increases, deviation becomes positive, which means that the change of direction is
482 following the direction of slope's aspect. These findings are in-line consistent with
483 trends described by Asteriou & Tsiambaos (2016), but the deviation of the actual
484 trajectory is significantly lower. This can be attributed to the different conditions (i.e.
485 block shape, slope material, slope roughness, incident velocity and angle, and scale)
486 between the experimental program conducted by Asteriou & Tsiambaos (2016) and
487 the Ponti rockfall event.

488 **7. Discussion – Conclusions**

489 UAV-enabled reconnaissance was successfully used for the identification of the
490 origin of the detached rock, the rockfall trajectory and the impact points on the slope,
491 and especially discerning the rolling and bouncing sections of
492 the trajectory. A UAV with an ultra-
493 high definition (UHD) camera was deployed to reach the inaccessible, steep and
494 partly vegetated uphill terrain. A high-resolution orthophoto of the rockfall trajectory, a
495 and a 10 cm DSM and a 2 m DTM were generated as prepared and, which formed
496 the basis for an analytical 2D kinematic analysis and a comparison with the
497 outcomes of 2D and 3D rockfall analysis software.

498 The initial velocity of the detached rock was estimated based on site conditions and
499 amplification of the ground acceleration due to topography. It was found that the

500 ~~estimation of the~~ initial velocity of the blocks plays a significant role in the accurate
501 re-production of the rockfall trajectory.

502 Based on the ~~analytical~~ computational analysis performed, it was found that the
503 coefficients of restitution cannot be directly connected to the material type, nor can
504 be considered material constants. The impact angle seems to ~~influence the pose a~~
505 ~~consistent effect on~~ normal COR, which has been also observed ~~also~~ in other recent
506 ~~relevant~~ studies, but has not been incorporated yet on analysis models.

507 It was proven impossible to replicate the actual trajectory of the rock fall by
508 performing a 2D rockfall analysis with the ~~recommended~~ set of parameters indicating
509 ~~recommended by the developers revealing some~~ limitations in the present
510 formulations. In an attempt to match the actual rock path to the analysis output, the
511 friction angle of the limestone slope was considered equal to zero. However, the
512 falling rock still rolled on the slope and stopped much earlier than its actual runout
513 distance while the impacts on the ground in the bouncing section of the trajectory
514 were considerably different in number and in location compared to the actual ones.

515 Using the 3D analysis software, and recommended input parameters, some rock
516 trajectories better approximated the actual trajectory ~~using the suggested values by~~
517 ~~the software developers,~~ indicating that the 3D analysis can be more accurate than
518 the 2D analysis.

519 Based on the aforementioned analyses it becomes evident that engineering
520 judgement and experience must accompany the usage of commercial rockfall
521 software in order to acquire realistic paths. One should never blindly use the
522 ~~recommended~~ suggested set of parameters since field performance can differ
523 significantly, as demonstrated by this case study.

524

525 **References**

- 526 1. Agliardi F, Crosta GB (2003) High resolution three-dimensional numerical
527 modelling of rockfalls. *International Journal of Rock Mechanics and Mining*
528 *Sciences* 40:455-471. doi: 10.1016/S1365-1609(03)00021-2
- 529 2. Asteriou P, Saroglou H, Tsiambaos G (2012). Geotechnical and kinematic
530 parameters affecting the coefficients of restitution for rock fall analysis.
531 *International Journal of Rock Mechanics and Mining Sciences* 54:103-113.
532 doi:10.1016/j.ijrmms.2012.05.029.
- 533 3. Asteriou P and Tsiambaos G. (2016). Empirical Model for Predicting Rockfall
534 Trajectory Direction. *Rock Mechanics and Rock Engineering* 49.3, pp. 927–
535 941.
- 536 4. Azzoni A, de Freitas MH (1995). Experimentally gained parameters, decisive
537 for rock fall analysis. *Rock Mechanics and Rock Engineering* 28:111-124. doi:
538 10.1007/BF01020064
- 539 5. Buzzi O, Giacomini A, Spadari M (2012) Laboratory investigation on high
540 values of restitution coefficients. *Rock Mechanics and Rock Engineering*
541 45:35-43
- 542 6. Crosta GB, Agliardi F (2004) Parametric evaluation of 3D dispersion of
543 rockfall trajectories. *Natural Hazards and Earth System Science* 4:583-598.
544 doi:10.5194/nhess-4-583-2004
- 545 7. Descoeurdes F, Zimmermann TH. Three-dimensional dynamic calculation of
546 rockfalls. In: *Proceedings of the 6th International Congress on Rock*
547 *Mechanics*. Montreal; 30 August -3 September 1987. p. 337–42.
- 548 8. Dorren, L.K.A., 2012. Rockyfor3D (v5.1) revealed - Transparent description of
549 the complete 3D rockfall model. ecorisQ paper, 31 p.
- 550 9. Ganas, A., Briole, P., Papathanassiou, G., Bozionelos, G., Avallone, A.,
551 Melgar, D., Argyrakis, P., Valkaniotis, S., Mendonidis, E., Moshou, A. and

- 552 Elias, P. (2015). A preliminary report on the Nov 17, 2015 M=6.4 South
553 Lefkada earthquake, Ionian Sea, Greece, Report to EPPO, December 4
554 2015.
- 555 10. Ganas A., Elias P., Bozionelos G., Papathanassiou G., Avallone A.,
556 Papastergios P. Valkaniotis S., Parcharidis I., Briole P. (2016). Coseismic
557 deformation, field observations and seismic fault of the 17 November 2015 M
558 = 6.5, Lefkada Island, Greece earthquake. *Tectonophysics* 687, pp. 210–222.
- 559 11. Giani GP. *Rock Slope Stability Analysis*. Rotterdam: Balkema A.A; 1992.
- 560 12. Giacomini A, Thoeni K, Lambert C, Booth S, Sloan SW (2012) Experimental
561 study on rockfall drapery systems for open pit highwalls. *International Journal*
562 *of Rock Mechanics and Mining Sciences* 56:171-181.
563 doi:10.1016/j.ijrmms.2012.07.030
- 564 13. Ferrari F, Giani GP, Apuani T (2013) Why can rockfall normal restitution
565 coefficient be higher than one? *Rendiconti Online Societa Geologica Italiana*
566 24
- 567 14. Heidenreich B (2004) Small- and half-scale experimental studies of rockfall
568 impacts on sandy slopes. Dissertation, EPFL.
- 569 15. ITSAK (2016). Preliminary presentation of the main recording of ITSAK –
570 OASP accelerometer network in Central Ionian. Earthquake M6.4 17/11/2015.
571 Thessaloniki, 11 pp.
- 572 16. Karakostas, V. G., Papadimitriou, E. E., and Papazachos, C. B. 2004.
573 Properties of the 2003 Lefkada, Ionian Islands, Greece, Earthquake Seismic
574 Sequence and Seismicity Triggering. *Bulletin of the Seismological Society of*
575 *America*, 94 (5), 1976–1981, October 2004
- 576 17. [Lindsay JB. 2016. Whitebox GAT: A case study in geomorphometric analysis.](#)
577 [Computers & Geosciences, 95: 75-84. DOI: 10.1016/j.cageo.2016.07.003](#)

- 578 18. Manousakis J., Zekkos D., Saroglou H., Clark M. (2016). Comparison of UAV-
579 enabled photogrammetry-based 3D point clouds and interpolated DSMs of
580 sloping terrain for rockfall hazard analysis. Proc. Int. Archives of the
581 Photogrammetry, Remote Sensing and Spatial Information Sciences, Vol.
582 XLII-2/W2, p. 71-78.
- 583 19. Marinou P, Tsiambaos G., 2002. Earthquake triggering rock falls affecting
584 historic monuments and a traditional settlement in Skyros Island, Greece.
585 Proc. of the Int. Symposium: Landslide risk mitigation and protection of
586 cultural and natural heritage, Kyoto, Japan, pp. 343-346.
- 587 20. Mavrouli O., Corominas J., Wartman J. (2009). Methodology to evaluate rock
588 slope stability under seismic conditions at Sol`a de Santa Coloma, Andorra.
589 Nat. Hazards Earth Syst. Sci., 9, 1763–1773. Micheletti N., Chandler J., Lane
590 S., 2015. Structure from Motion (SfM) Photogrammetry. British Society for
591 Geomorphology. *Geomorphological Techniques*, Chap. 2, Sec. 2.2 (2015)
- 592 22. Papathanassiou, G., Valkaniotis, S., Ganas, A. and Pavlides, S. 2012. GIS-
593 based statistical analysis of the spatial distribution of earthquake-induced
594 landslides in the island of Lefkada, Ionian Islands, Greece, Landslides,
595 Journal of the International Consortium on Landslides, DOI 10.1007/s10346-
596 012-0357-1
- 597 23. Papazachos B.C., Papadimitriou E.E., Kiratzi A.A., Papazachou C.B., Louvari
598 E.K. 1998. Fault plane solutions in the Aegean sea and the surrounding area
599 and their tectonic implication. Bull Geof Teor Appl 39(3), 199–218.
- 600 24. Paronuzzi P. (2009) Field Evidence and Kinematical Back-Analysis of Block
601 Rebounds: The Lavone Rockfall, Northern Italy. *Rock Mech Rock Eng*,
602 42:783–813

- 603 25. Richards LR, Peng B, Bell DH (2001) Laboratory and field evaluation of the
604 normal Coefficient of Restitution for rocks. Proceedings of ISRM Regional
605 Symposium EUROCK2001:149-155
- 606 26. RocScience, 2004. Rocfall Manual.
- 607 27. Rondoyanni Th., Mettos A., Paschos P., Georgiou Ch. 2007. Neotectonic
608 map of Greece, scale 1:100.000, Lefkada sheet. I.G.M.E., Athens.
- 609 28. Saroglou, H. 2013. Rockfall hazard in Greece. Bulletin of the Geological
610 Society of Greece, vol. XLVII, no3, 1429-1438.
- 611 29. Saroglou, H., Marinou, V., Marinou, P., Tsiambaos, G. 2012. Rockfall hazard
612 and risk assessment: an example from a high promontory at the historical site
613 of Monemvasia, Greece. Natural Hazards and Earth System Sciences, 12,
614 1823–1836. doi:10.5194/nhess-12-1823-2012.
- 615 30. Snavely N., Seitz S.N., Szeliski R., 2008. Modeling the world from internet
616 photo collections. *International Journal of Computer Vision* 80: 189-210.
- 617 31. Spadari M, Giacomini A., Buzzi O., Fityus S., Giani G.P.(2011). In situ rockfall
618 testing in New South Wales, Australia. *Int J Rock Mech Mining Sci*, 49, pp.
619 84–93.
- 620 32. Volkwein, A., Schellenberg, K., Labiouse, V., Agliardi, F., Berger, F., Bourrier,
621 F., Dorren, L. K. A., Gerber, W., and Jaboyedoff, M., 2011. Rockfall
622 characterisation and structural protection – a review, *Nat. Hazards Earth Syst.*
623 *Sci.*, 11, 2617–2651, doi:10.5194/nhess-11-2617-2011.
- 624 35. Westoby M.J., Brasington J., Glasser N.F., Hambrey M.J., Reynolds J.M.,
625 2012. ‘Structure-from-Motion’ photogrammetry: A low-cost, effective tool for
626 geoscience applications. *Geomorphology* 179 (2012) 300-314.
- 627 36. Wyllie, D. C. (2014). Calibration of rock fall modeling parameters.
628 *International Journal of Rock Mechanics and Mining Sciences* 67: 170-180

629 37. Zekkos D., Clark M., Cowell K., Medwedeff W., Manousakis J., Saroglou H.
630 Tsiambaos G. (2017). Satellite and UAV-enabled mapping of landslides
631 caused by the November 17th 2015 M_w 6.5 Lefkada earthquake. Proc. 19th Int.
632 Conference on Soil Mechanics and Geotechnical Engineering, Seoul, [17-22](#)
633 [September -2017](#).
634

634

TABLES

635

Table 1. Accelerometer recordings

Component	Acceleration (cm/sec ²)	Velocity (cm/sec)	Displacement (cm)
NS-comp	363	59.3	21.27
EW-comp	327	34.1	14.01
Z-comp	256	17.7	6.56

636

637 Table 2. Impact points characteristics

Impact point	X (m)	Y (m)	app_dip (°)	$\Delta\phi$ (°)	e (°)
1	287.63	338	39.0	0	0
2	298.38	329.68	16.3	33	0
3	305.48	324.5	27.9	27	-1
4	321.54	314.83	41.0	11.6	0.5
5	365.34	287.6	30.4	11.9	0.3
6	373.32	284.85	39.7	10.6	1.8
7	425.1	261.64	14.7	6.6	-1.3
8	464.43	251.13	18.4	33.3	0.8
9	472.06	248.81	14.0	19.1	2.3
10	495.29	243.81	7.5	52.3	0.9
11	515.31	240.8	7.9	51	0.6
12	535.56	238.31	9.1	46.7	3
13	562.11	232.22	8.7	47.3	2.1
14	605.51	211.12	16.9	25.6	-1.7
15	619.1	204.48	27.1	4.6	-3
16	639.13	196.96	21.2	8	4.7
17	662.41	184	23.3	28.5	5.2
18	688.4	169.3	27.4	0.3	-2.5
19	712.23	157.67	25.4	0.5	0.1
20	745.28	143.16	21.9	0.5	-0.1
21	762.9	137.01	22.0	0.7	2
22	789.23	125.98	21.6	1.4	-0.8
23	801.53	132.75	8.4	0.2	0.1

638 Table 3. Parabolic paths characteristics for the minimum release velocity

Segment	$\Delta x(m)$	$\Delta y(m)$	$\theta_{cr} (^{\circ})$	$v_{r,min}$	v_{impact}	a_i	v_{COR}	n_{COR}	t_{COR}
1-2	10.75	-8.33	26.8	7.19	13.19	44.5	0.55	0.71	0.31
2-3	7.1	-5.18	25.7	5.95	9.51	27.8	0.63	0.90	0.53
3-4	16.07	-9.66	31.5	9.45	12.68	9.6	0.75	3.86	0.38
4-5	43.79	-27.23	27.7	15.46	23.13	23.3	0.67	1.57	0.26
5-6	7.98	-2.75	35.7	7.47	10.49	14.9	0.71	2.52	0.30
6-7	51.78	-23.21	34.8	18.15	21.61	31.7	0.84	1.54	0.26
7-8	39.33	-10.5	35.9	17.23	24.01	36.1	0.72	0.94	0.56
8-9	7.63	-2.32	35.9	7.45	10.54	41.1	0.71	0.87	0.55
9-10	23.23	-5	40.5	13.58	13.12	30.7	1.03	1.65	0.70
10-11	20.02	-3.01	41.1	13.00	11.57	24.2	1.12	2.06	0.82
11-12	20.25	-2.49	40.9	13.26	11.22	17.6	1.18	2.94	0.82
12-13	26.55	-6.1	38.0	14.40	14.25	28.5	1.01	1.55	0.78
13-14	43.41	-21.1	32.9	16.33	25.70	40.9	0.64	0.64	0.63
14-15	13.59	-6.64	30.7	9.13	12.81	25.1	0.71	1.24	0.53
15-16	20.03	-7.52	33.8	11.67	15.42	29.8	0.76	1.33	0.42
16-17	23.27	-12.96	31.9	11.59	15.89	28.5	0.73	1.22	0.50
17-18	25.99	-14.7	29.9	12.20	20.11	30.9	0.61	0.95	0.42
18-19	23.83	-11.63	32.2	12.08	17.10	27.9	0.71	1.30	0.40
19-20	33.05	-14.51	33.6	14.55	20.62	32.1	0.71	1.14	0.43
20-21	17.62	-6.15	34.5	11.08	11.99	18.4	0.92	2.44	0.54
21-22	26.33	-11.03	35.1	13.11	16.33	27.3	0.80	1.47	0.49
22-23	12.3	6.77	58.1	14.30	13.97	48.9	1.02	1.34	0.28

639

640

640 Table 4. Restitution parameters for Rockyfor3D

Geological formation/ other	Mean n_{COR}	MOH			Soil type (Rockyfor3D)
		rg70	rg20	rg10	
Scree ($\emptyset < \sim 10$ cm), or medium compact soil with small rock fragments	0.33	0.03	0.05	0.05	3
Talus slope ($\emptyset > \sim 10$ cm), or compact soil with large rock fragments	0.38	0.05	0.1	0.2	4
Talus with fallen boulders	0.42	0.15	0.15	0.2	4.1
Bedrock with thin weathered material	0.43	0	0.05	0.1	5
Asphalt road	0.35	0	0	0	7

641

FIGURES

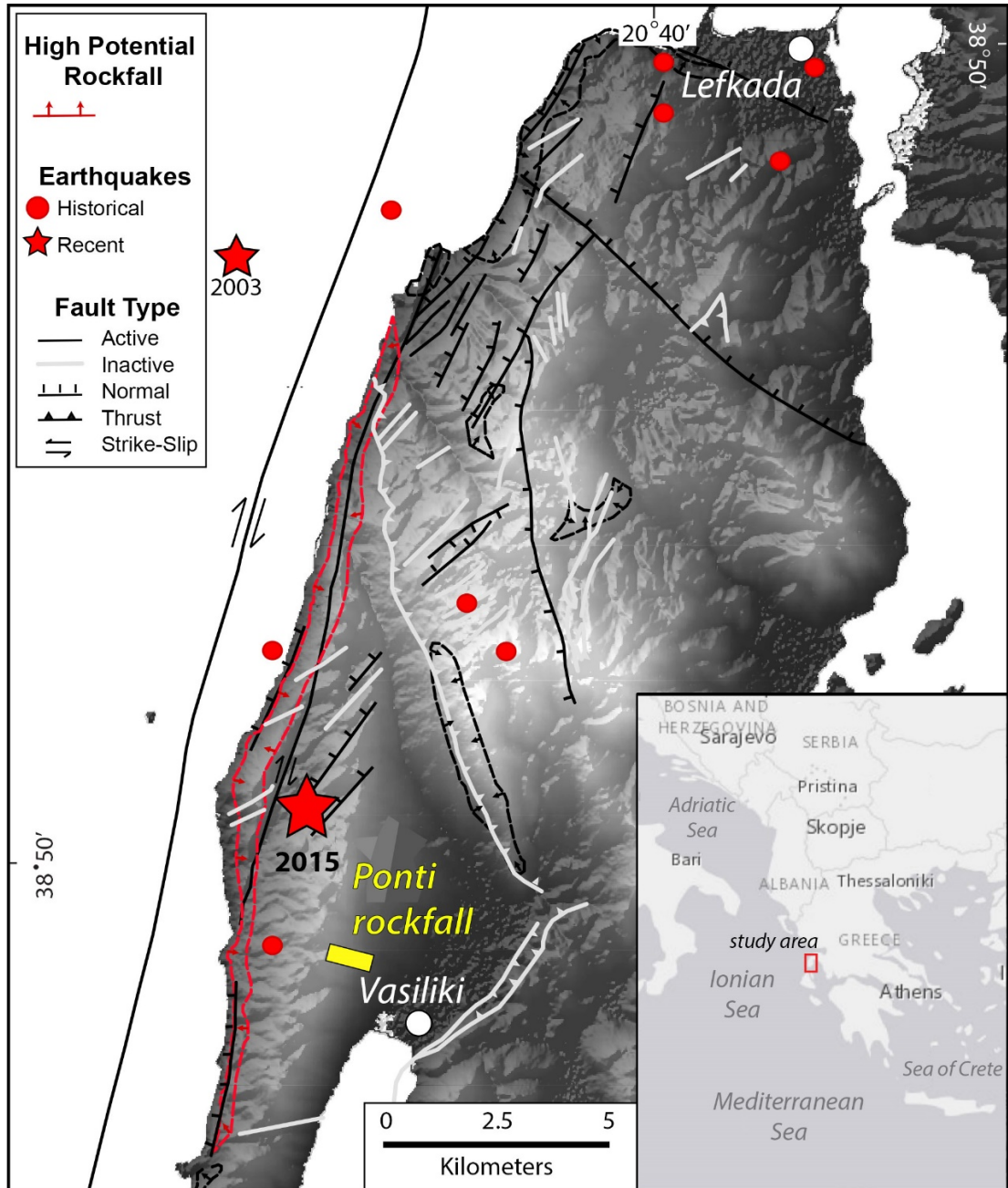


Figure 1. Map of Lefkada Island, Greece with location of study site (Ponty) and epicenters of recent earthquakes (stars) in 2003 (M_w 6.2) and 2015 (M_w 6.5), as well as historical ones (circles) Map also shows faults and high potential rockfall areas as identified by Rondoyanni et al. (2007).

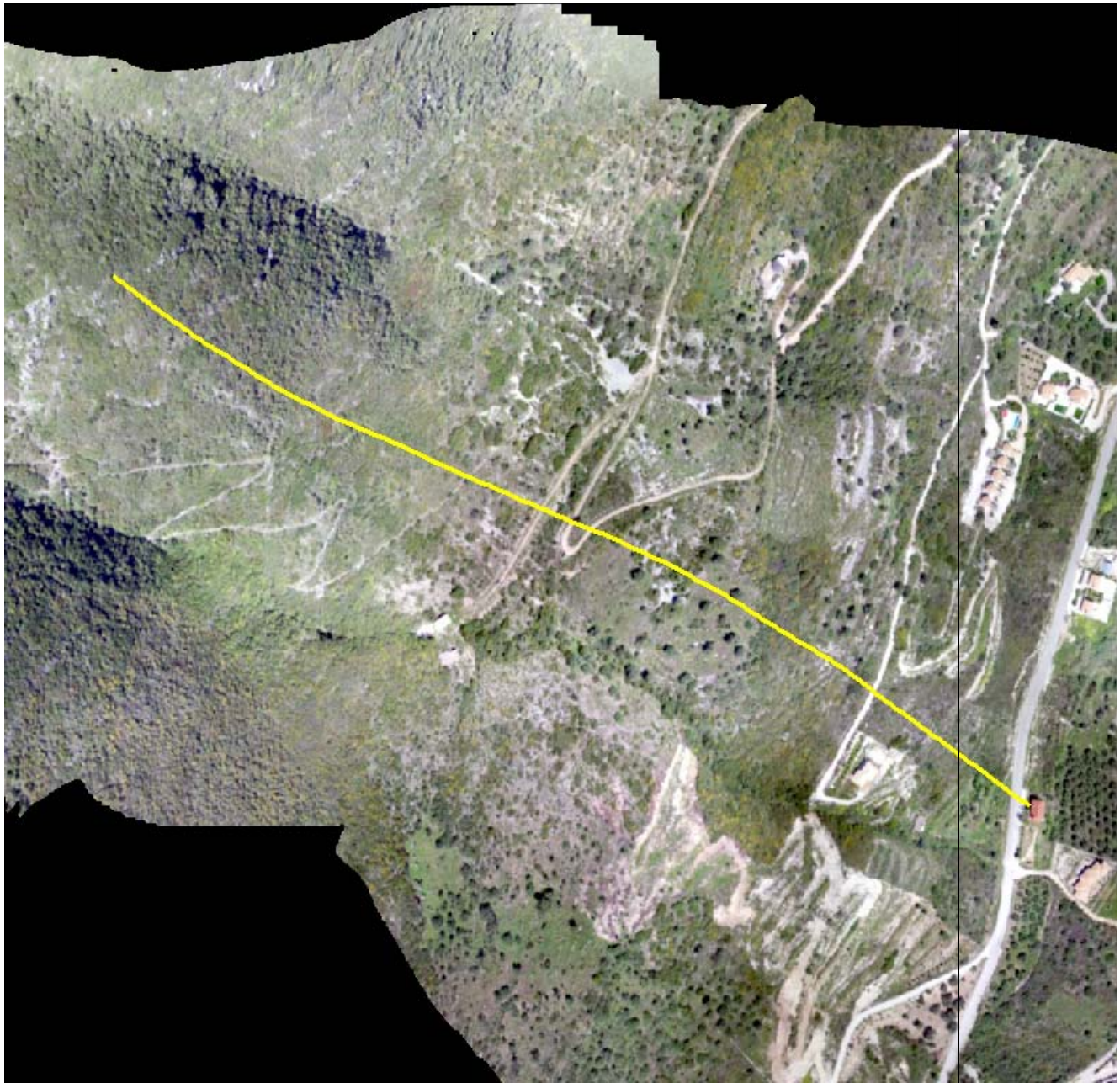


Figure 2. Orthophoto of case study. The total length of the trajectory shown with a yellow line, is 800 m.



Figure 3. Impact of rock on house in Ponti, Lefkada, Greece.

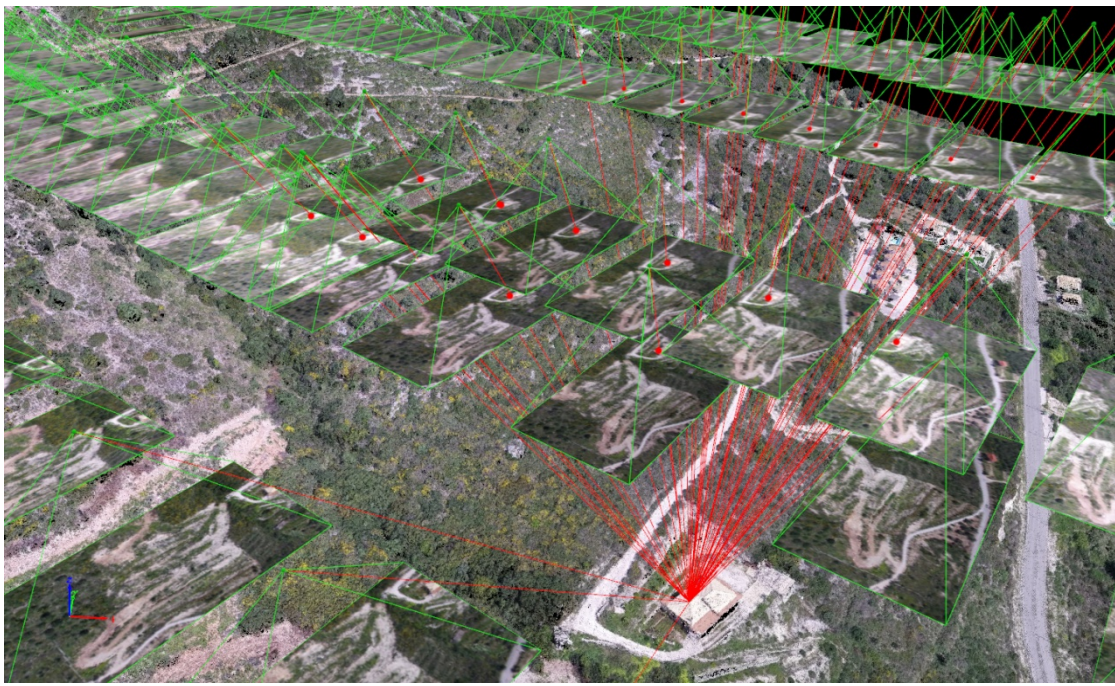
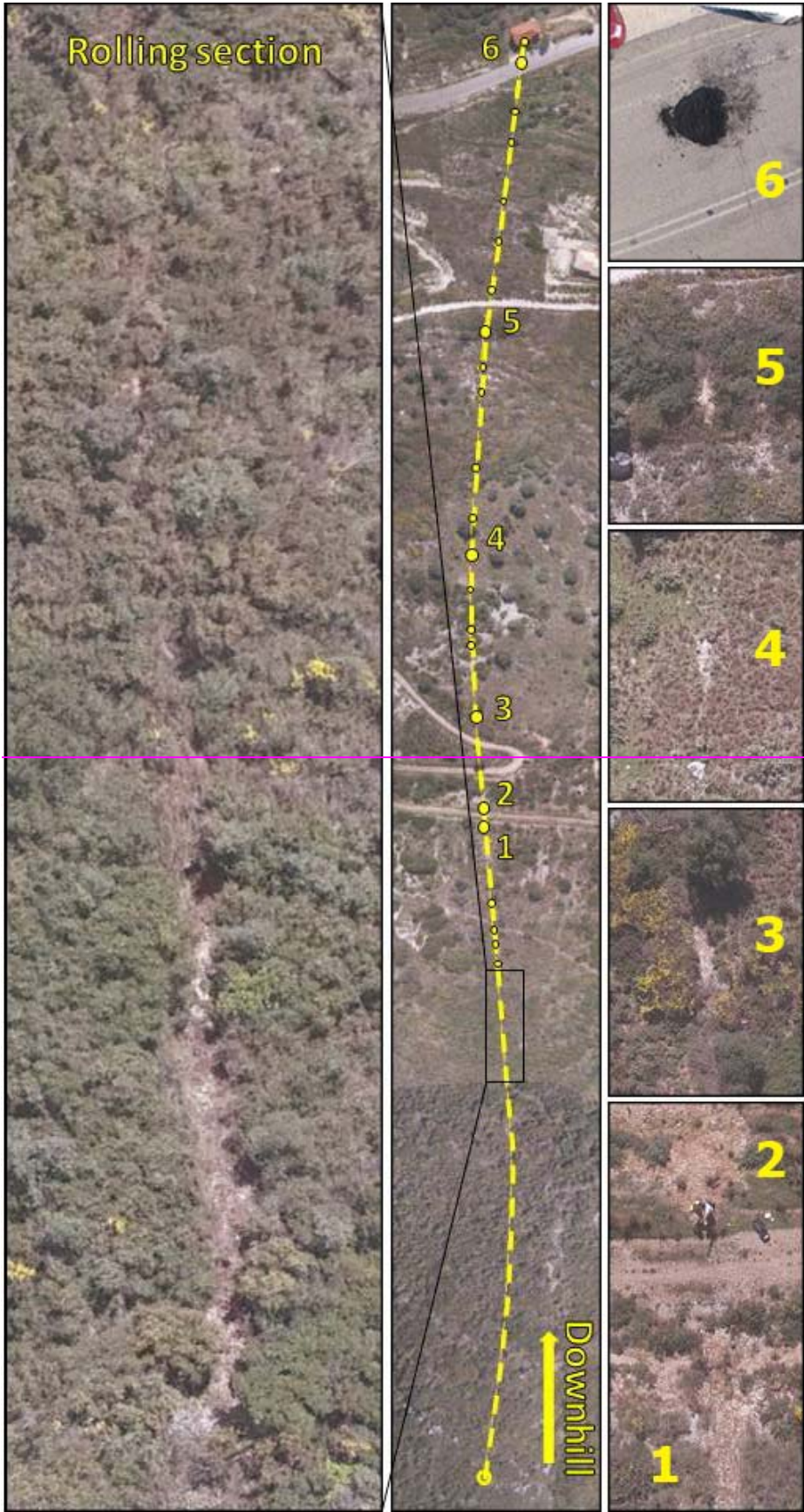


Figure 4. Schematic illustrating the overlap between pictures in the study site using SfM methodology.



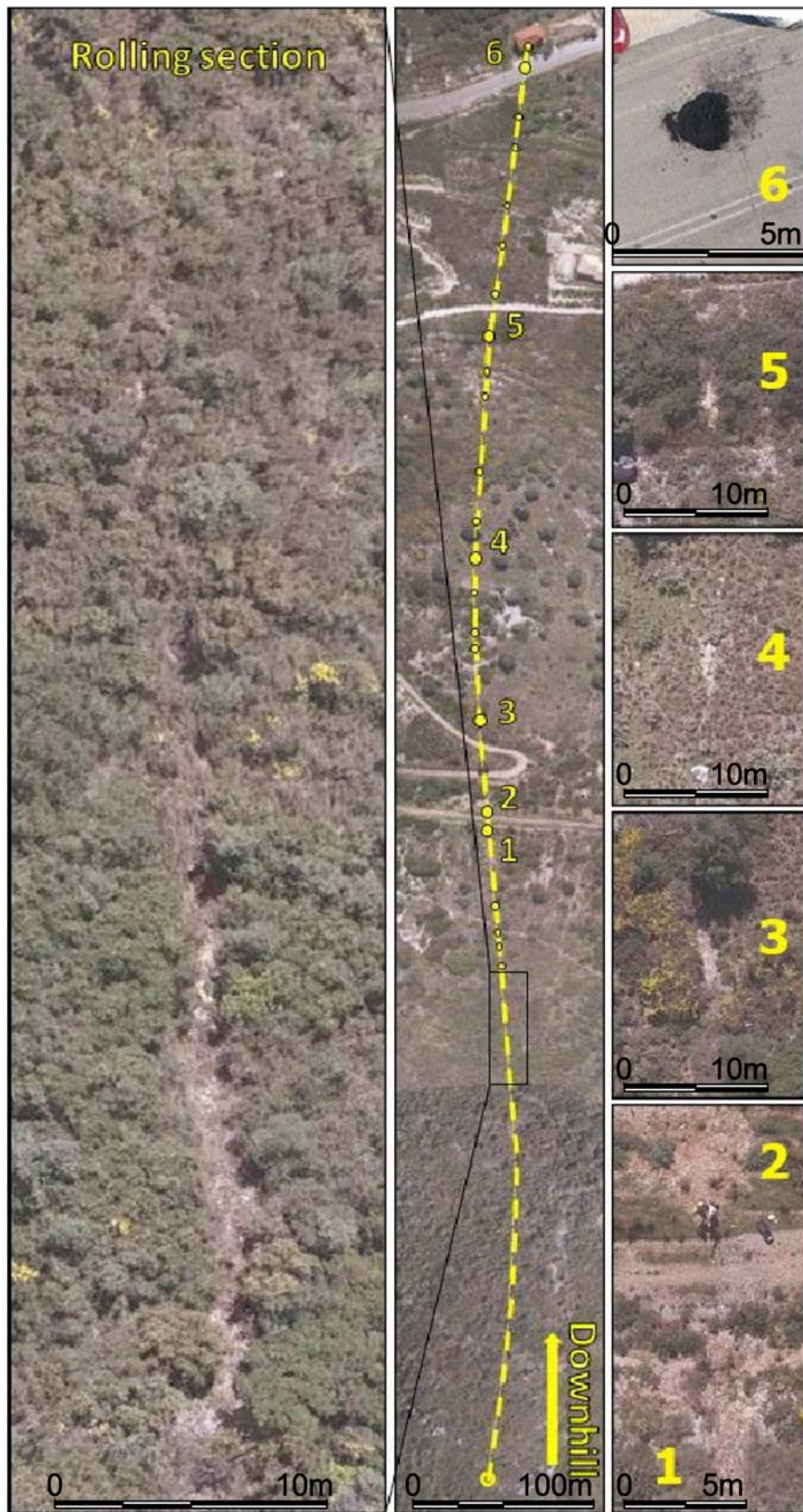


Figure 5. Top view orthophoto denoting rolling section, bouncing positions and indicative close-ups of impact points.

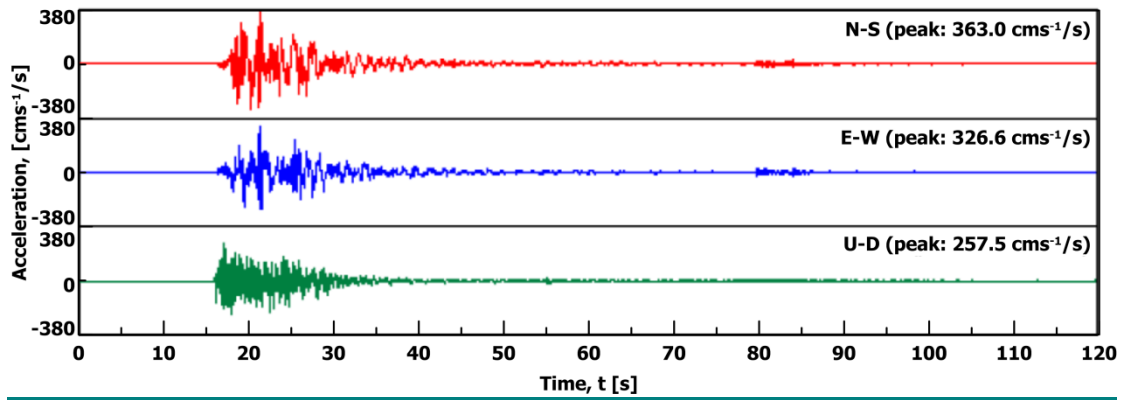


Figure 6. Acceleration [time history](#) recording at Vassiliki site (ITSAK, 2016)

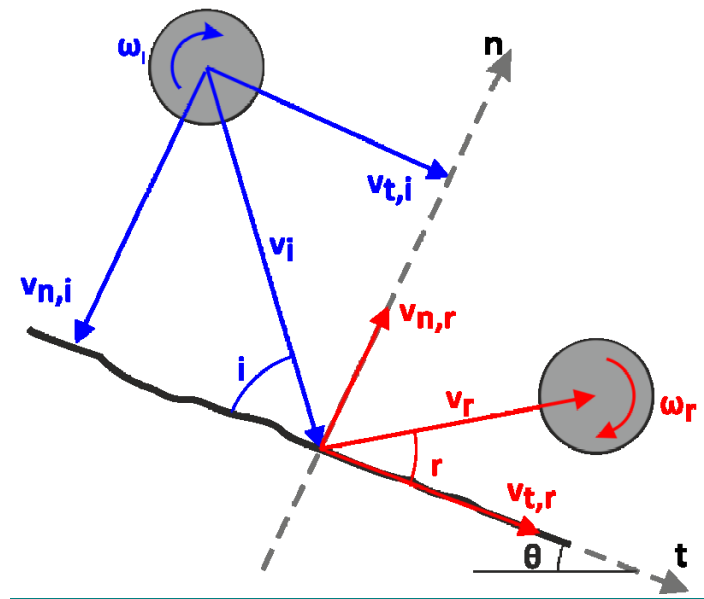


Figure 7. Coefficients of restitution

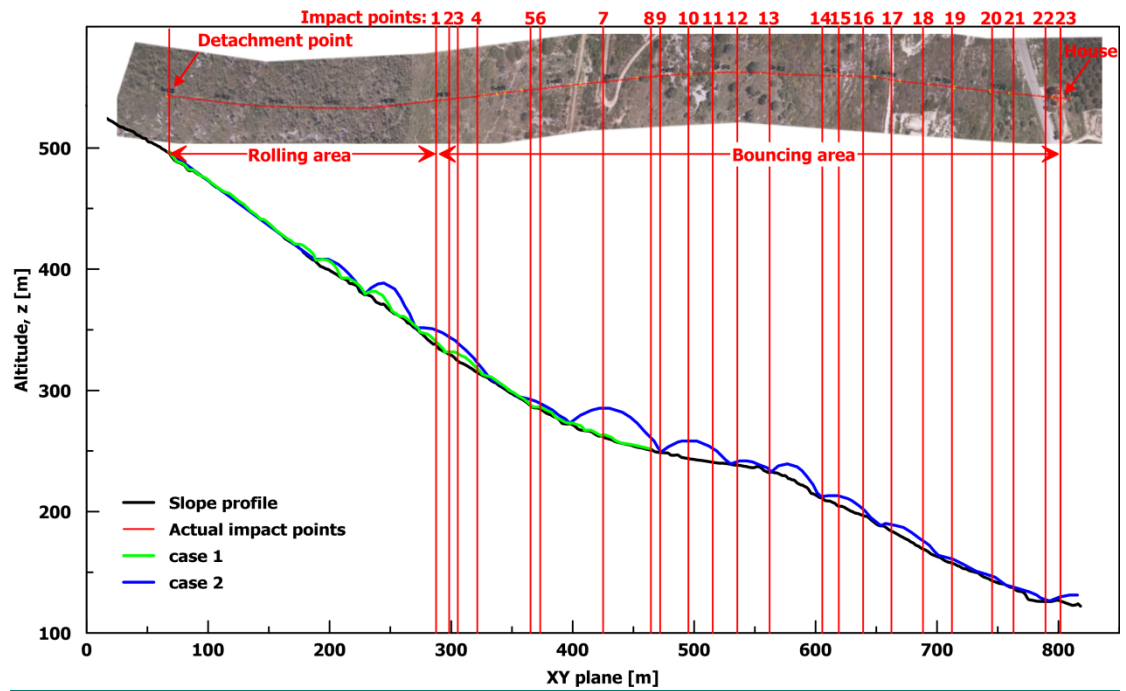


Figure 8. Plan view and cross section along block's path (units in m); 2D rockfall trajectory analysis results are plotted with green and blue line

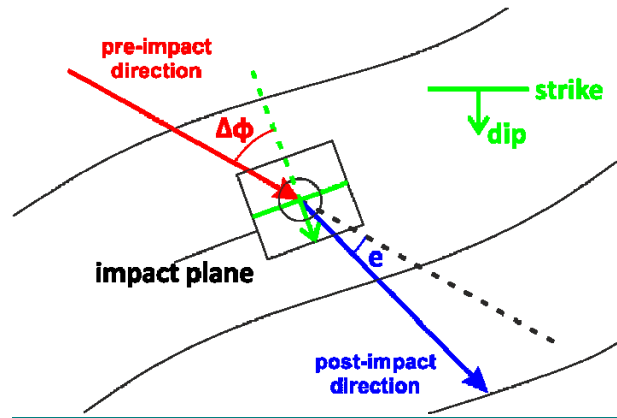


Figure 9 : Out of plane geometry

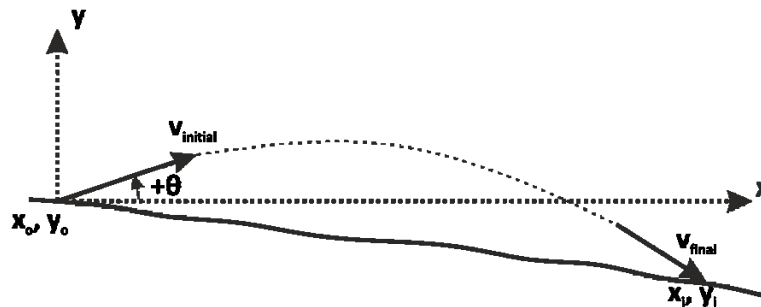


Figure 10. Parabolic segment

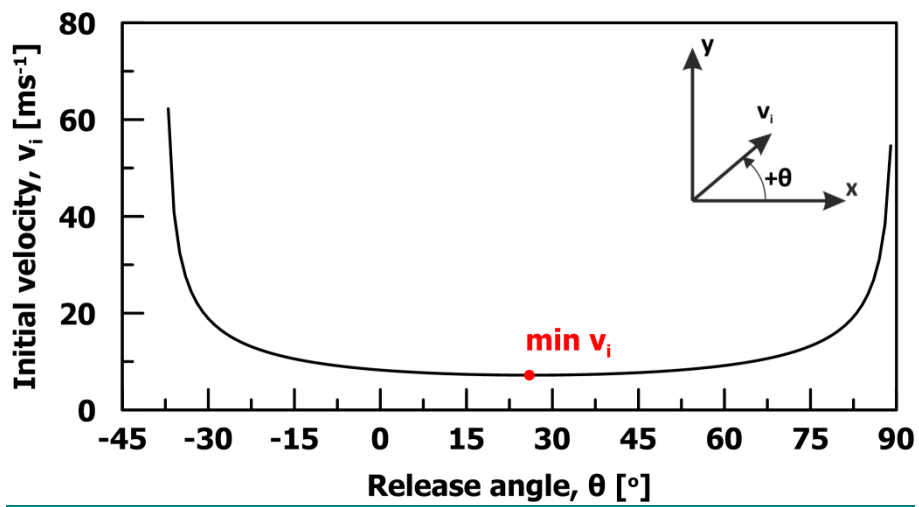


Figure 11. Release angle versus initial velocity for the first parabolic section ($\delta x=10.75\text{m}$, $\delta y=8.33\text{m}$)

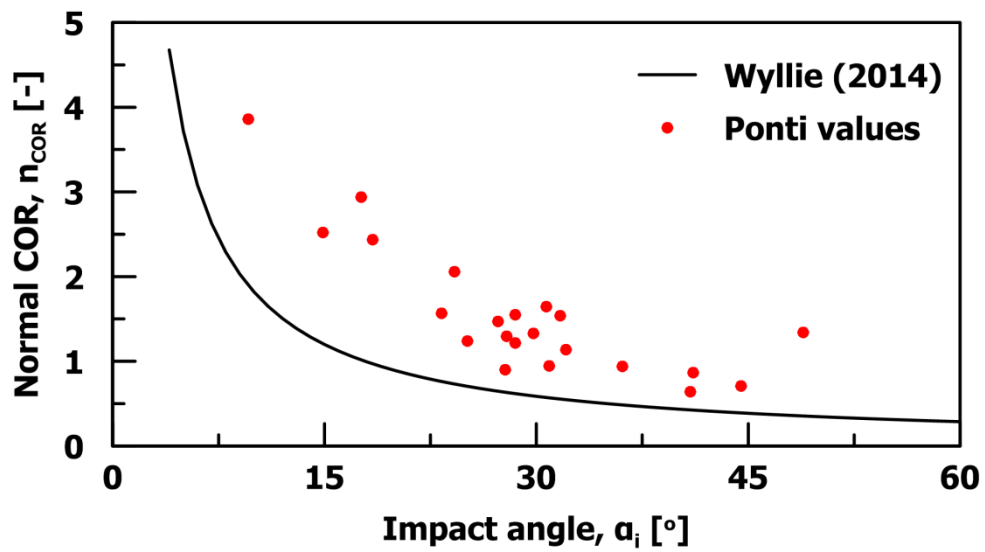


Figure 12. Normal COR versus impact angle

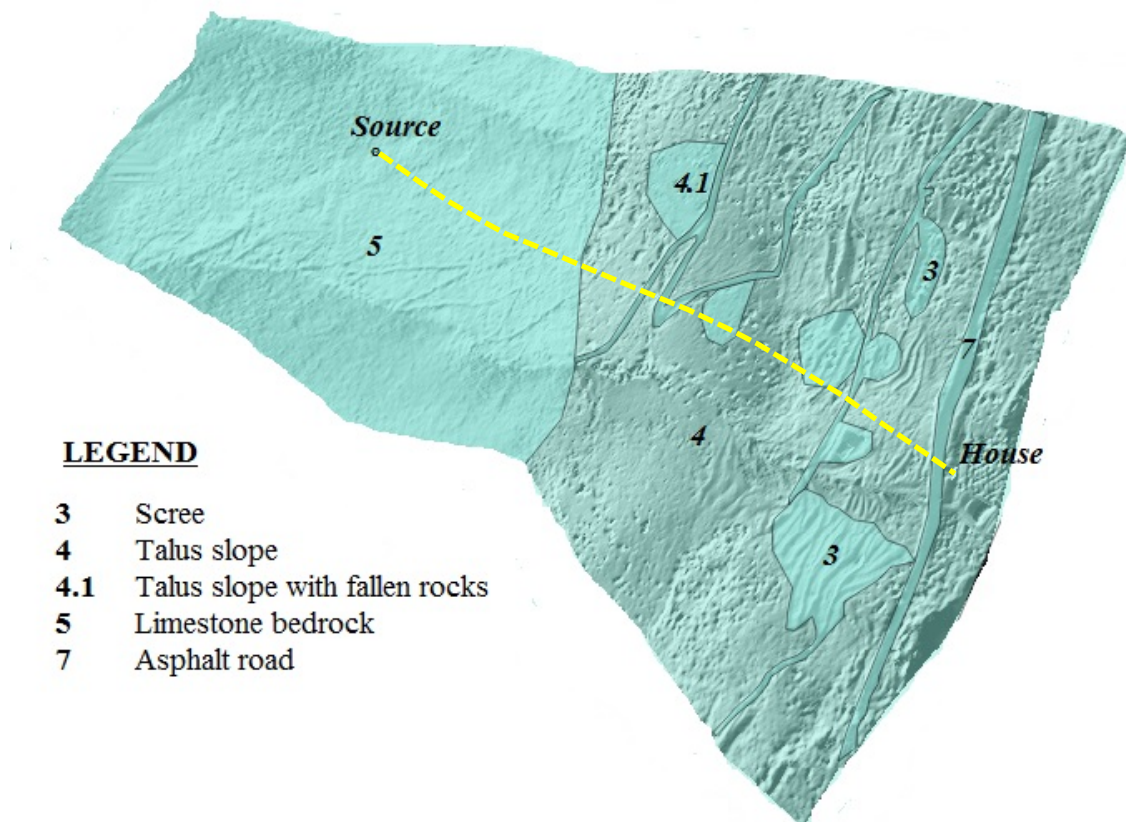


Figure 13. Soil types for 3D rockfall analysis (according to Rockyfor3D). Yellow path of trajectory is 800 m.

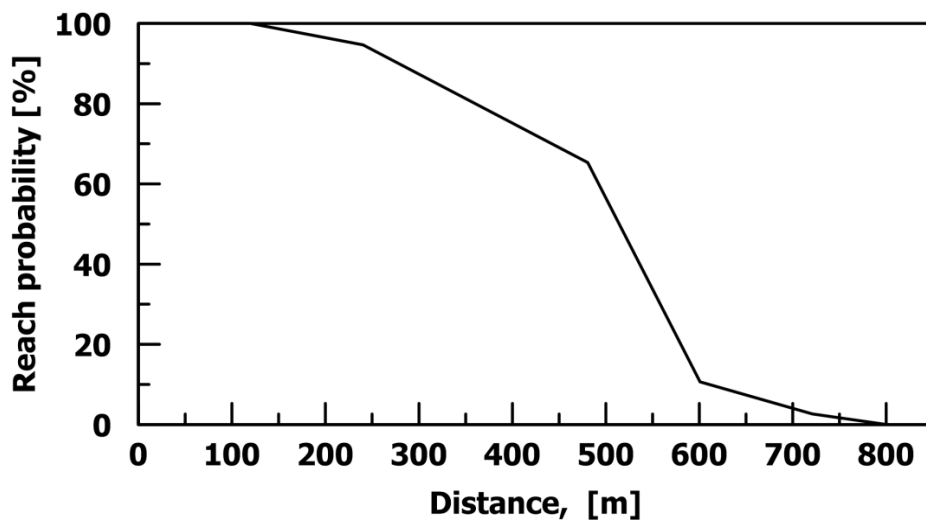


Figure 14. Reach probability graph calculated from 3D rockfall analysis

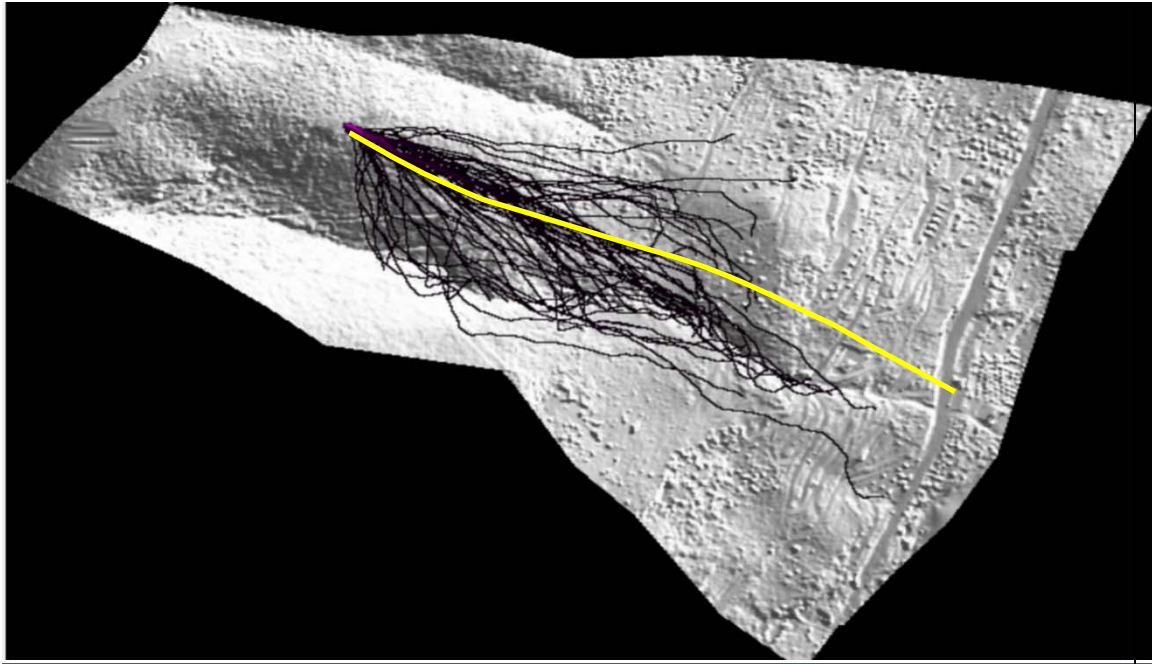


Figure 15. 3D trajectory analysis (from RockyFor3D analysis). Yellow line shows the actual trajectory. Black lines show the simulated trajectory.

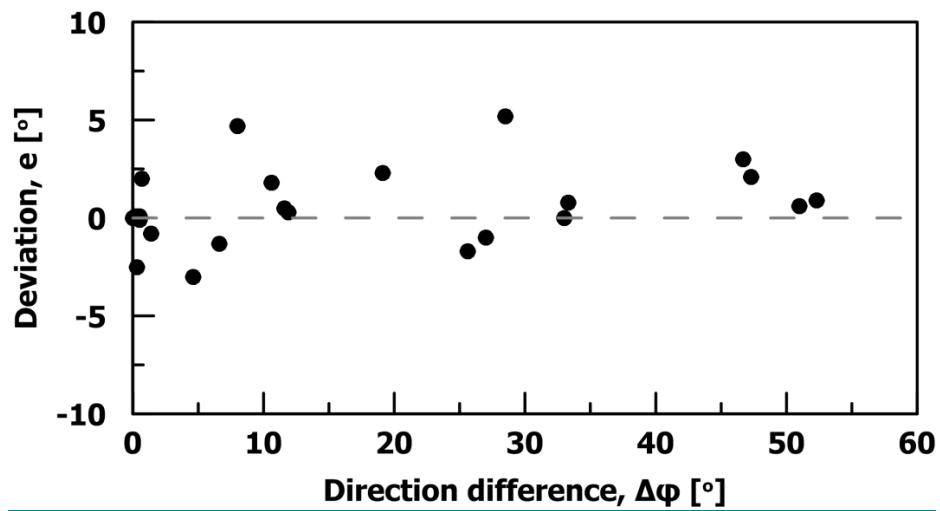


Figure 16. Deviation as a function of direction difference.